June 2008

Efficient Reduction of CO_2 in a Solid Oxide Electrolyzer

F. Bidrawn
University of Pennsylvania

G. Kim
University of Pennsylvania

G. Corre
University of St. Andrews

J. T.S. Irvine
Unversity of St. Andrews

John M. Vohs
University of Pennsylvania, vohs@seas.upenn.edu

See next page for additional authors

Reprinted from *Electrochemical and Solid-State Letters*, 2008, Vol. 11, No. 9, pp. B167–B170, July 2008.

Efficient Reduction of CO_2 in a Solid Oxide Electrolyzer

Abstract

The electrolysis of CO_2 has been examined in a solid oxide electrolyzer (SOE) using a ceramic electrode based on $La_{0.8}Sr_{0.2}Cr_{0.5}Mn_{0.5}O_3$ (LSCM), infiltrated into a yttria-stabilized zirconia scaffold together with 0.5 wt % Pd supported on 5 wt % $Ce_{0.48}Zr_{0.48}Y_{0.04}O_2$. An SOE with this electrode exhibited a total cell impedance of 0.36 Ω cm^2 at 1073 K for operation in $CO–CO_2$ mixtures. An additional benefit is that the $CO–CO_2$ electrode was shown to be redox stable, with LSCM exhibiting good conductivity in both oxidizing and reducing environments, so that the cell can operate in pure CO_2.

Comments

Reprinted from *Electrochemical and Solid-State Letters*, 2008, Vol. 11, No. 9, pp. B167–B170, July 2008.

Author(s)

F. Bidrawn, G. Kim, G. Corre, J. T.S. Irvine, John M. Vohs, and Raymond J. Gorte

Electrochemical and Solid-State Letters, **11** (9) B167-B170 (2008)
1099-0062/2008/11(9)/B167/4/$23.00 © The Electrochemical Society

Efficient Reduction of CO_2 in a Solid Oxide Electrolyzer

F. Bidrawn,[a] G. Kim,[a] G. Corre,[b] J. T. S. Irvine,[b,*,z] J. M. Vohs,[a,*] and R. J. Gorte[a,*,z]

[a]*Department of Chemical and Biomolecular Engineering, University of Pennsylvania, Philadelphia, Pennsylvania 19104, USA*
[b]*School of Chemistry, University of St. Andrews, Fife KY16 9ST, United Kingdom*

The electrolysis of CO_2 has been examined in a solid oxide electrolyzer (SOE) using a ceramic electrode based on $La_{0.8}Sr_{0.2}Cr_{0.5}Mn_{0.5}O_3$ (LSCM), infiltrated into a yttria-stabilized zirconia scaffold together with 0.5 wt % Pd supported on 5 wt % $Ce_{0.48}Zr_{0.48}Y_{0.04}O_2$. An SOE with this electrode exhibited a total cell impedance of 0.36 Ω cm^2 at 1073 K for operation in CO–CO_2 mixtures. An additional benefit is that the CO–CO_2 electrode was shown to be redox stable, with LSCM exhibiting good conductivity in both oxidizing and reducing environments, so that the cell can operate in pure CO_2.
 [DOI: 10.1149/1.2943664]

Manuscript submitted April 11, 2008; revised manuscript received May 18, 2008. Published June 20, 2008.

When the economy is based on renewable energy resources, such as wind and solar, the major source of H_2 for chemical production and energy storage will be from the electrolysis of water. The ability to reduce CO_2 efficiently by a similar process could also play a role in reducing greenhouse gas emissions and moving us toward a more sustainable economy.[1] CO produced in this manner could be used in chemical production or reacted with H_2 to produce liquid fuels via the Fischer–Tropsch reaction.[2]

Solid oxide electrolyzers (SOEs), which are essentially solid oxide fuel cells (SOFCs) operated in reverse, are capable of higher water electrolysis efficiencies compared to solution-based electrolysis cells because they operate at higher temperatures (>925 K). The higher operating temperatures result in a lower Nernst potential, the thermodynamic potential required for water splitting, and in lower electrode overpotentials.[3] (The electrode overpotential is the difference between the actual electrode potential and the Nernst potential, and is a measure of the lost efficiency in the cell.) SOEs also differ from low-temperature, solution-based electrolyzers in that the electrolyte membrane conducts oxygen anions, rather than protons. The material most often used for the electrolyte is yttria-stabilized zirconia (YSZ), a material that is a good oxygen-anion conductor and an electronic insulator. In an SOE, the cathode (the fuel-side electrode) reaction for water electrolysis is the electrochemical dissociation of steam to produce H_2 and O^{2-} anions, Reaction 1, while recombination of the oxygen ions to O_2, Reaction 2, occurs at the anode (the air-side electrode)

$$H_2O + 2e^- \rightarrow O^{2-} + H_2 \quad [1]$$

$$O^{2-} \rightarrow 2e^- + 1/2O_2 \quad [2]$$

By analogy to Reaction 1, the reduction of CO_2 can also be carried out at the fuel-side electrode using Reaction 3

$$CO_2 + 2e^- \rightarrow O^{2-} + CO \quad [3]$$

Finally, note that the Nernst potentials for the electrolysis of H_2O and CO_2 are virtually identical.

There are a few reports for the electrochemical reduction of CO_2 to CO in SOEs.[4-6] Most of these have focused on O_2 production for space missions and have employed expensive bulk Pt electrodes that would not be practical for large-scale CO_2 electrolysis as would be required for sustainable chemical and fuel production. Furthermore, the overpotentials for the Pt electrodes used in these studies were very high, so that the efficiency for CO_2 reduction was low.

In conventional SOE used for steam electrolysis, the fuel-side electrode is a composite of Ni and YSZ,[7-9] the same material that is used in SOFCs for oxidation of H_2. In principle, Ni–YSZ electrodes can be used for CO_2 electrolysis[10] but they suffer from several important limitations. First, while Ni–YSZ electrodes are efficient for H_2 oxidation, electrode overpotentials for CO oxidation are much higher.[11] Indeed, a highly optimized SOFC that was able to produce 1.8 W/cm^2 when H_2 was the fuel produced less than 0.3 W/cm^2 on a 44% CO–56% CO_2 mixture at 1073 K.[12] When SOFCs are operated on syngas, a mixture of CO and H_2, the oxidation of CO proceeds primarily through the water–gas-shift reaction, $CO + H_2O \rightarrow H_2 + CO_2$, with H_2 oxidation still the primary electrochemical reaction.[11,12] Second, there are concerns about the stability of Ni–YSZ composites in a CO–CO_2 environment. Ni carbonyls are highly volatile,[13] making it important to choose operating conditions for which carbonyl formation is less favorable. Ni is also a superb catalyst for the Boudouard reaction, $2CO \rightarrow C + CO_2$,[14,15] so that operation would be limited to higher temperatures and CO_2:CO ratios to avoid equilibrium conditions favorable for this reaction. Finally, Ni–YSZ composites are severely damaged by reoxidation.[16] Because Ni would be oxidized by pure CO_2, it would be necessary to ensure that the feed to any CO_2 electrolyzer contained sufficient CO or H_2 to make the gas composition reducing over all parts of the electrode.

Our groups have recently demonstrated that it is possible to achieve a very high performance with an electrode made from 45 wt % $La_{0.8}Sr_{0.2}Cr_{0.5}Mn_{0.5}O_3$ (LSCM), 0.5 wt % Pd, and 5 wt % ceria infiltrated into a porous YSZ scaffold.[17] In this composite electrode, LSCM provides electronic conductivity, YSZ provides ionic conductivity, and the Pd–ceria mixture enhances the catalytic activity for fuel oxidation. An SOFC with this fuel–electrode composition exhibited maximum power densities at 1073 K of 1.1 and 0.71 W/cm^2 in humidified (3% H_2O) H_2 and methane, respectively, even though the cell had a relatively thick, 60 μm YSZ electrolyte. The composite electrode was also stable to oxidation and reduction cycles, showing conductivity under both oxidizing and reducing conditions. Finally, none of the materials used in the LSCM-based electrode forms vapor-phase carbonyls, and none is a good catalyst for carbon formation by the Boudouard reaction. These attributes make this electrode design a good candidate for use in a CO_2 SOE system.

In this paper, we describe the performance characteristics for CO_2 electrolysis of an SOE with a fuel electrode based on LSCM. The results demonstrate that this electrode is very efficient for the electrochemical reduction of CO_2.

Experimental

Cells were fabricated by first preparing a three-layer YSZ wafer, consisting of two porous layers separated by a dense electrolyte layer, 65 μm thick as previously described.[17-19] The three-layer ceramic wafers were produced by laminating three green ceramic tapes, synthesized by tape casting, with pore formers in the two outer tapes. The laminated green tapes were fired to 1773 K to produce the final ceramic structures. The porous layer on one side of

* Electrochemical Society Active Member.
z E-mail: jtsi@st-andrews.ac.uk; gorte@seas.upenn.edu

the electrolyte was 300 μm thick YSZ (~65% porous) and was used as the scaffold for the air-side electrode, while the other porous layer was 60 μm thick YSZ (~65% porous) and was used as the scaffold for the fuel-side electrode. Porosity in the 300 μm layer was obtained using a mixture of graphite and polystyrene pore formers (the latter was used to introduce larger pores), while the thinner porous layer used only graphite.

The addition of 45 wt % LSCM to the porous fuel-side layer was the next step in cell fabrication. The impregnating solution was prepared by adding $La(NO_3)_3 \cdot 6H_2O$ (Alfa Aesar, ACS 99.9%), $Sr(NO_3)_2$ (Alfa Aesar, ACS 99.0%), $Cr(NO_3)_3 \cdot 9H_2O$ (Alfa Aesar, ACS 98.5%), and $Mn(NO_3)_2 \cdot xH_2O$ (Alfa Aesar, ACS 99.98%) to distilled water in the correct molar ratios, then mixing this with citric acid (≥99.5%, Aldrich) to produce a solution with a citric-acid:metal-ion ratio of 2:1. After infiltrating the porous layer with this solution, the ceramic wafer was heated in air to 750 K to decompose the nitrate ions and the citric acid. This procedure was repeated until the desired weight loading of LSCM was achieved. Finally, the wafer was heated in air to 1473 K to produce the perovskite structure.

After forming the LSCM in the porous layer, the $(La_{0.8}Sr_{0.2}FeO_3)$ LSF–YSZ air-side electrodes were synthesized by impregnating the 300 μm thick layer with an aqueous solution containing $La(NO_3)_3 \cdot 6H_2O$, $Sr(NO_3)_2$, and $Fe(NO_3)_3 \cdot 9H_2O$, to a loading of 40 wt % LSF, followed by calcination to 1123 K.[18] The impedance of LSF–YSZ electrodes prepared in this way is between 0.1 and 0.15 Ω cm^2 at 973 K and is independent of current density under both fuel-cell and electrolyzer conditions. Following the addition of LSF, 0.5 wt % Pd and 5 wt % of the mixed oxide, $Ce_{0.48}Zr_{0.48}Y_{0.04}O_2$ (CZY), were added as catalysts to the LSCM-containing layer by addition of the nitrate salts and heating in air to 750 K. Pd supported on ceria–zirconia is known to be highly active for oxidation catalysis,[20] and Y doping of the ceria–zirconia maintains the mixed oxide as a single-phase material following high-temperature treatments.[21] The addition of an oxidation catalyst was found to be essential for achieving high electrode performance.[17]

For testing, cells were attached to an alumina tube with a ceramic adhesive (Aremco, Ceramabond 552). Electrical connections were achieved using Ag paste and Ag wire at both the air and fuel electrodes. The gas to the fuel-side electrode was either humidified (10% H_2O) H_2 or a mixture of CO and CO_2, with the concentration controlled by the relative flow rates of the gases. The air electrode was simply exposed to the ambient air. Impedance spectra were measured at open circuit in the galvanostatic mode with a frequency range of 0.1 Hz to 100 kHz and a 10 mV ac perturbation using a Gamry Instruments potentiostat. The active area of the cells, equal to the area of the fuel electrode, was 0.35 cm^2; but the area of the electrolyte and of the air electrode was approximately 1 cm^2.

Results and Discussion

A complete description of the LSCM–YSZ[17] electrode microstructure is given elsewhere. What this earlier work showed is that the infiltration process produces a remarkable morphology, with a thin porous layer of electronically conductive LSCM covering the surface of the YSZ scaffold. Infiltration of the $Pd/Ce_{0.48}Zr_{0.48}Y_{0.04}O_2$ catalyst into the LSCM pores then adds the necessary catalytic sites. This microstructure appears to be critical for achieving high performance by providing a mixed conducting substrate with a large, catalytically active, three-phase boundary. The electrode was demonstrated to be thermally stable on cycling up to at least 1173 K.

Figure 1 shows a comparison of the cell performance with the fuel-side electrode exposed to 90% H_2–10% H_2O and 90% CO–10% CO_2 mixtures at 973 K. In this figure, oxidation of H_2 and CO is indicated by positive currents and reduction of H_2O and CO_2 by negative currents. The cell potential at zero current was 1.05 V in H_2–H_2O and 1.07 V in CO–CO_2, which is close to the calculated Nernst potentials for these fuel compositions when the opposite electrode is exposed to ambient air. Because the feeds to the fuel side of the cell were dilute in both H_2O and CO_2, the overpotentials in electrolysis are higher than those under fuel-cell conditions. With the H_2–H_2O mixture, a current density of 1.14 A/cm^2 was obtained at a cell potential of 0.5 V, while the corresponding electrolysis current density at 1.5 V was only 0.64 A/cm^2. With CO–CO_2 mixtures, the corresponding current densities at 0.5 and 1.5 V were 0.75 and 0.34 A/cm^2, respectively.

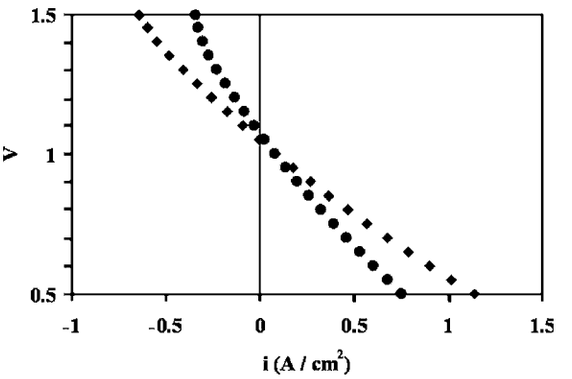

Figure 1. V-i polarization curves for 10% H_2O–90% H_2 (♦) and 10% CO_2–90% CO (●) mixtures at 973 K. Negative currents correspond to electrolysis of H_2O or CO_2. The cell composition was as follows: 40 wt % LSF in YSZ|YSZ(65 μm)| 0.5 wt % Pd, 5 wt % CZY, and 45 wt % LSCM in YSZ.

The corresponding open-circuit impedance spectra, Fig. 2, provide insight into the origin of the overpotential losses while operating in the electrolysis mode. As expected, a significant fraction of the cell losses was ohmic and attributable to the internal resistance drop in the 65 μm YSZ electrolyte. The measured ohmic losses, determined from the high-frequency intercept with the abscissa, were 0.37 Ω cm^2 for operation in H_2 and H_2O and 0.35 Ω cm^2 for operation in CO and CO_2, in good agreement with the calculated resistance of 0.35 Ω cm^2 expected for the 65 μm electrolyte, using reported YSZ conductivities.[22] The nonohmic losses, determined from the length of the arc under the impedance curves, were 0.19 Ω cm^2 for operation in H_2–H_2O and 0.6 Ω cm^2 for operation in CO–CO_2. Losses for the LSF–YSZ air electrode are estimated to be between 0.1 and 0.15 Ω cm^2 at 973 K,[18] suggesting that the fuel electrode losses in H_2–H_2O are approximately 0.1 Ω cm^2 and those in CO–CO_2 mixtures are 0.5 Ω cm^2.

Figures 3 and 4 show the voltage–current density (V-i) relationships for the cell during electrochemical reduction of CO_2 and oxidation of CO as a function of the CO:CO_2 ratio in the fuel at 973 and 1073 K, respectively. When pure CO_2 is fed to the fuel-side

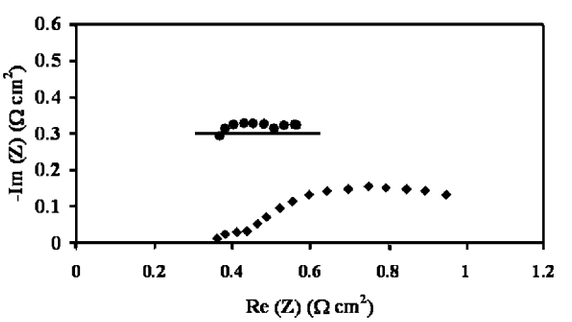

Figure 2. Cole–Cole plots, measured at the open-circuit potentials or OPCs if it shortened, for 10% H_2O–90% H_2 (●) and 10% CO_2–90% CO (♦) mixtures at 973 K. The cell composition was as follows: 40 wt % LSF in YSZ|YSZ(65 μm)| 0.5 wt % Pd, 5 wt % CZY, and 45 wt % LSCM in YSZ.

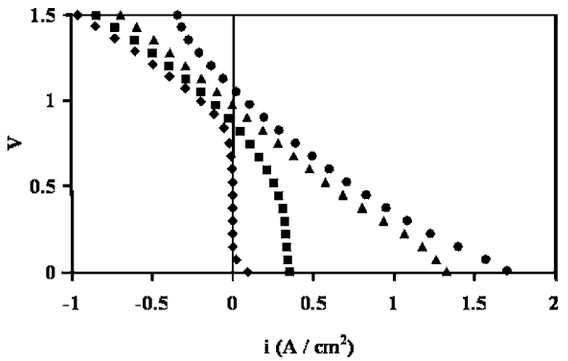

Figure 3. V-i polarization curves for mixtures of CO_2 and CO at 973 K. Negative currents correspond to electrolysis of CO_2. 100% CO_2–0% CO (♦); 90% CO_2–10% CO (■); 50% CO_2–50% CO (▲); 10% CO_2–90% CO (●). The cell composition was as follows: 40 wt % LSF in YSZ|YSZ(65 μm)| 0.5 wt % Pd, 5 wt % CZY, and 45 wt % LSCM in YSZ.

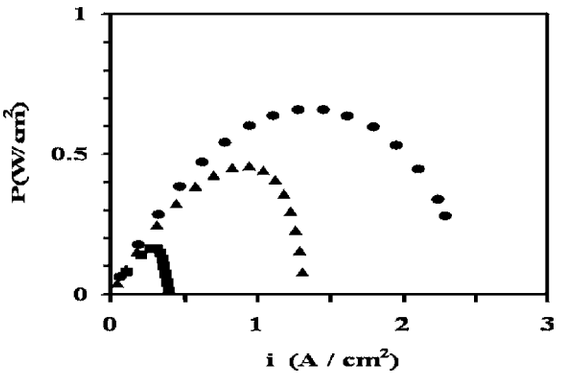

Figure 5. The power density as a function of current density for the cell operating in the fuel-cell mode on CO–CO_2 mixtures at 1073 K: 90% CO_2–10% CO (■); 50% CO_2–50% CO (▲); 10% CO_2–90% CO (●). The cell composition was as follows: 40 wt % LSF in YSZ|YSZ(65 μm)| 0.5 wt % Pd, 5 wt % CZY, and 45 wt % LSCM in YSZ.

electrode, the open-circuit potential (OCP) is close to zero. (These are obviously conditions for which a Ni–YSZ electrode would undergo oxidation.) The cell potential rises to ~0.8 V as CO is produced by CO_2 reduction. At 1.5 V, the reduction current reaches 0.96 A/cm^2 at 973 K and 1.8 A/cm^2 at 1073 K. At 973 K for a CO_2:CO ratio of 9:1, the OCP is 0.87 V and increases with decreasing the CO_2:CO ratio. The slope of the V-i curve remains nearly the same as that for pure CO_2, however, as long as there is sufficient CO_2 to avoid diffusional limitations. Diffusion limitations are almost certainly the reason for the increase in the slope at higher current densities. The nearly constant slopes, approximately 0.63 Ω cm^2 at 973 K and 0.36 Ω cm^2 at 1073 K, reflect the fact that the electrode impedances are nearly current-independent so long as the diffusion of CO_2 (for CO_2 reduction) or CO (for CO oxidation) is not limiting. Because 65 μm YSZ electrolyte contributes to the increased slope of these lines, 0.35 Ω cm^2 at 973 K and 0.15 Ω cm^2 at 1073 K,[22] significant improvements could be made by using a thinner electrolyte.

Next, we consider how the LSCM-based electrode in the present study compares to the best Ni–YSZ electrodes. Because the only available CO_2 electrolysis data on cells with Ni–YSZ electrodes are for much higher temperatures, 1223 K,[10] we instead compare the performance of our cells operating as a fuel cell. As mentioned in the beginning, a highly optimized SOFC with a Ni–YSZ anode and a 10 μm thick electrolyte produced less than 0.3 W/cm^2 on a 44% CO–56% CO_2 mixture at 1073 K, even though it was capable of producing 1.8 W/cm^2 on 100% H_2 at this temperature.[12] Figure 5, which shows the power density as a function of current density for our cell operating in the fuel-cell mode in various CO–CO_2 mixtures, demonstrates that our cell achieved 0.45 W/cm^2 in a 50% CO_2–50% CO mixture at this temperature, even with a 65 μm electrolyte. Clearly, the performance of these LSCM-based electrodes in CO–CO_2 mixtures is excellent.

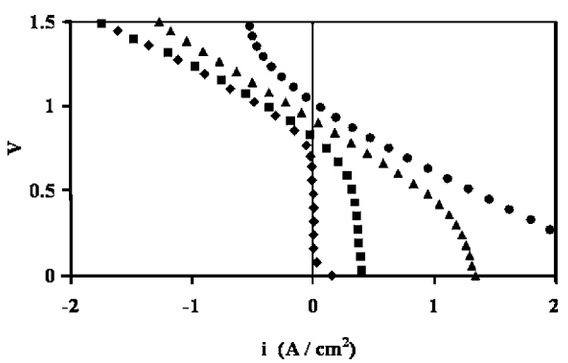

Figure 4. V-i polarization curves for mixtures of CO_2 and CO at 1073 K. Negative currents correspond to electrolysis of CO_2. 100% CO_2–0% CO (♦); 90% CO_2–10% CO (■); 50% CO_2–50% CO (▲); 10% CO_2–90% CO (●). The cell composition was as follows: 40 wt % LSF in YSZ|YSZ(65 μm)| 0.5 wt % Pd, 5 wt % CZY, and 45 wt % LSCM in YSZ.

Conclusion

We have demonstrated that it is possible to reduce CO_2 electrochemically with an efficiency that is similar to that which can be achieved for H_2O electrolysis. This result suggests that reduction of CO_2 by electrolysis in an SOE is feasible and could play a role in the development of sustainable and nongreenhouse-gas-emitting energy and fuel cycles which use renewable energy sources such as wind and solar to produce chemicals and liquid fuels.

Acknowledgments

This work was funded by the U.S. Department of Energy's Hydrogen Fuel Initiative (grant DE-FG02-05ER15721) and by the Office of Naval Research, grant N00014-07-1-0046. We also thank EPSRC-GB for support.

University of St. Andrews assisted in meeting the publication costs of this article.

References

1. C. M. Sanchez-Sanchez, V. Montiel, D. A. Tryk, A. Aldaz, and A. Fujishima, *Pure Appl. Chem.*, **73**, 1917 (2001).
2. C. H. Bartholomew and R. J. Farrauto, *Fundamentals of Industrial Catalytic Processes*, 2nd ed., p. 398, John Wiley & Sons, Hoboken, NJ (2006).
3. G. Parkinson, *Chem. Eng. Prog.*, **102**, 7 (2006).
4. T. Yamamoto, D. A. Tryk, A. Fujishima, and H. Ohata, *Electrochim. Acta*, **47**, 3327 (2002).
5. K. R. Sridhar and B. T. Vaniman, *Solid State Ionics*, **93**, 321 (1997).
6. G. Tao, K. R. Sridhar, and C. L. Chan, *Solid State Ionics*, **175**, 621 (2004).
7. O. A. Marina, L. R. Pederson, M. C. Williams, G. W. Coffey, K. D. Meinhardt, D. D. Nguyen, and E. C. Thomsen, *J. Electrochem. Soc.*, **154**, B452 (2007).
8. A. Hauch, S. H. Jensen, J. B. Bilde-Sorensen, and M. Mogensen, *J. Electrochem. Soc.*, **154**, A619 (2007).
9. S. Elangovan, J. J. Hartvigsen, and L. J. Frost, *Int. J. Appl. Ceram. Technol.*, **4**, 109 (2007).
10. S. H. Jensen, P. H. Larsen, and M. Mogensen, *Int. J. Hydrogen Energy*, **32**, 3253 (2007).
11. O. Costa-Nunes, R. J. Gorte, and J. M. Vohs, *J. Power Sources*, **141**, 241 (2005).
12. Y. Jiang and A. V. Virkar, *J. Electrochem. Soc.*, **150**, A942 (2003).
13. K. Morikawa, T. Shirasaki, and M. Okada, *Adv. Catal.*, **20**, 98 (1969).
14. M. L. Toebes, J. H. Bitter, A. J. van Dillen, and K. P. de Jong, *Catal. Today*, **76**, 33 (2002).
15. E. Perry Murray, T. Tsai, and S. A. Barnett, *Nature (London)*, **400**, 649 (1999).

16. M. Cassidy, G. Lindsay, and K. Kendall, *J. Power Sources*, **61**, 189 (1996).
17. G. Kim, G. Corre, J. T. S. Irvine, J. M. Vohs, and R. J. Gorte, *Electrochem. Solid-State Lett.*, **11**, B16 (2008).
18. W. S. Wang, M. D. Gross, J. M. Vohs, and R. J. Gorte, *J. Electrochem. Soc.*, **154**, B439 (2007).
19. M. D. Gross, J. M. Vohs, and R. J. Gorte, *J. Electrochem. Soc.*, **154**, B694 (2007).
20. A. Trovarelli, *Catal. Rev. - Sci. Eng.*, **38**, 439 (1996).
21. G. Kim, M. D. Gross, W. Wang, J. M. Vohs, and R. J. Gorte, *J. Electrochem. Soc.*, **155**, B360 (2008).
22. K. Sasaki and J. Maier, *Solid State Ionics*, **134**, 303 (2000).